

VAE²: Preventing Posterior Collapse of Variational Video Predictions in the Wild

Yizhou Zhou,¹ Chong Luo,² Xiaoyan Sun,² Zheng-Jun Zha,¹ Wenjun Zeng²

¹University of Science Technology of China

²Microsoft Research Asia

zyz0205@mail.ustc.edu.cn zhazj@ustc.edu.cn

{xysun, cluo, wezeng}@microsoft.com

Abstract

Predicting future frames of video sequences is challenging due to the complex and stochastic nature of the problem. Video prediction methods based on variational auto-encoders (VAEs) have been a great success, but they require the training data to contain multiple possible futures for an observed video sequence. This is hard to be fulfilled when videos are captured in the wild where any given observation only has a determinate future. As a result, training a vanilla VAE model with these videos inevitably causes posterior collapse. To alleviate this problem, we propose a novel VAE structure, dubbed VAE-in-VAE or VAE². The key idea is to explicitly introduce stochasticity into the VAE. We treat part of the observed video sequence as a random transition state that bridges its past and future, and maximize the likelihood of a Markov Chain over the video sequence under all possible transition states. A tractable lower bound is proposed for this intractable objective function and an end-to-end optimization algorithm is designed accordingly. VAE² can mitigate the posterior collapse problem to a large extent, as it breaks the direct dependence between future and observation and does not directly regress the determinate future provided by the training data. We carry out experiments on a large-scale dataset called Cityscapes, which contains videos collected from a number of urban cities. Results show that VAE² is capable of predicting diverse futures and is more resistant to posterior collapse than the other state-of-the-art VAE-based approaches. We believe that VAE² is also applicable to other stochastic sequence prediction problems where training data are lack of stochasticity.

Introduction

Video prediction finds many applications in robotics and autonomous driving, such as action recognition(Zhou et al. 2018), planning(Thrun et al. 2006), and object tracking(Guo et al. 2017). Initially, video prediction was formulated as a reconstruction problem (Ranzato et al. 2014) where the trained model regresses a determinate future for any given observation. However, real-world events are full of stochasticity. For example, a person standing may sit down, jump up, or even fall down at the next moment. A deterministic model is not capable of predicting multiple possible futures, but such capability is tremendously desired by intelligent

agents as it makes them aware of different possible consequences of their actions in real applications. In order to bring stochasticity into video prediction, methods based on autoregressive models (Oord, Kalchbrenner, and Kavukcuoglu 2016), generative adversarial networks (GANs) (Goodfellow et al. 2014; Mirza and Osindero 2014), and variational auto-encoders (VAEs)(Kingma and Welling 2013) have been proposed. Among these, VAE-based methods have received the most attention and they are referred as variational video prediction (Babaeizadeh et al. 2017).

Variational video prediction learns a latent variable model that maximizes the likelihood of the data. A key to the success of variational video prediction is that the training dataset should provide multiple futures for observed frames. Not surprisingly, VAE-based video prediction methods have been using synthetic videos or scripted videos¹ for training. These videos can provide multiple futures as desired, but they only cover a small subset of real-world scenarios. In order to build a practically applicable video prediction model, it is necessary to train it with non-scripted real-world videos such as videos captured in the wild. However, such kind of videos are usually determinate, which means only one of many possible futures is available. This situation will easily collapse a VAE model. As Fig. 1(a) shows, if there is always a unique future v corresponding to each observation I , the hidden code z becomes trivial due to the inference preference property(Chen et al. 2016). In such a case, VAE loses the capability to predict diverse futures.

VAEs are known to suffer from posterior collapse due to various reasons such as the ‘optimization challenges’(Bowman et al. 2015; Razavi et al. 2019). Although many approaches (Higgins et al. 2017; Alemi et al. 2017; Goyal et al. 2017; Razavi et al. 2019; Bowman et al. 2015) have been proposed to mitigate the problem, they hold the basic assumption that the training data have a stochastic nature. To our best knowledge, none of the previous work has looked into the model collapse problem caused by the determinate training data in video prediction. The intuition behind our solution is to explicitly inject stochasticity into the VAEs. As illustrated in Fig. 1(b), we intentionally set aside a part of the observed video sequence I^s and treat it as a ran-

¹A human actor or robot conducts predefined activities in well-controlled environment.

dom transition state that bridges its past and future. By doing so, we can maximize the likelihood of a Markov Chain over the sequence under all possible transition states. Such formulation converts the likelihood that only relies on the observed data pairs (I, v) into an expectation which contains extra dependence on the distribution of the entire dataset.

However, this new formulation contains an expectation term and a likelihood term which are both intractable. To tackle it, we first derive a practical lower bound which can be optimized with a vanilla VAE structure, and then use another VAE to approximate the remaining intractable part in this lower bound. In addition, we find that the two objective functions for the two VAEs can be merged into a single expression in practice. This greatly saves the efforts to do iterative optimization. As a result, we can innovatively derive a nested VAE structure. We name this structure VAE-in-VAE, or VAE² in short. VAE² can be optimized in an end-to-end manner.

In a nutshell, the contributions of this work are: 1) We propose a novel VAE² framework to explicitly inject stochasticity into the VAE to mitigate the posterior collapse problem caused by determinate training data. 2) We turn the objective function tractable and develop an efficient end-to-end optimization algorithm. 3) We make evaluations on non-scripted real-world video prediction as well as a simple number sequence prediction task. Both quantitative and qualitative results demonstrate the efficacy of our method.

Related Work

The video prediction problem can be addressed by either deterministic or non-deterministic models. Deterministic models directly reconstruct future frames with recurrent neural networks(Ranzato et al. 2014; Oh et al. 2015; Srivastava, Mansimov, and Salakhudinov 2015; Villegas et al. 2017; Finn, Goodfellow, and Levine 2016; Lu, Hirsch, and Scholkopf 2017) or feed-forward networks(Jia et al. 2016; Vondrick and Torralba 2017; Liu et al. 2017; Walker, Gupta, and Hebert 2015). The reconstruction loss assumes a deterministic environment. Such models cannot capture the stochastic nature in real world videos and usually result in an averaged prediction over all possibilities.

Non-deterministic models can be further classified into autoregressive models, GANs, and VAEs. In pixel-level autoregressive models(Oord, Kalchbrenner, and Kavukcuoglu 2016), spatiotemporal dependencies are jointly modeled, where each pixel in the predicted video frames fully depends on the previously predicted pixel via chain rule (Kalchbrenner et al. 2017). Although autoregressive model can directly construct video likelihood through full factorization over each pixel, it is impractical due to its high inference complexity. Besides, it has been observed to fail on globally coherent structures(Razavi et al. 2019) and generate very noisy predictions (Babaeizadeh et al. 2017). GANs(Goodfellow et al. 2014) and conditional GANs (c-GANs)(Mirza and Osindero 2014) are also employed for stochastic video prediction, for their capability to generate data close to the target distribution. GAN-based approaches can predict sharp and realistic video sequences(Vondrick, Pirsiavash, and Tor-

ralba 2016), but is prone to model collapse and often fails to produce diverse futures(Lee et al. 2018).

VAE-based models have received the most attention among the non-deterministic models. In particular, conditional VAEs (c-VAEs) have been shown to be able to forecast diverse future actions a single static image (Walker et al. 2016; Xue et al. 2016). c-VAEs have also been used to predict diverse future sequences from an observed video sequence (Babaeizadeh et al. 2017; Lee et al. 2018; Denton and Fergus 2018; Minderer et al. 2019). In some of these approaches, human body skeleton(Minderer et al. 2019) and dense trajectory(Walker et al. 2016) are incorporated in addition to the RGB frames to enhance the prediction quality. Besides, RNN-based encoder-decoder structures such as LSTM(Hochreiter and Schmidhuber 1997) has also been employed for long-term predictions(Wichers et al. 2018). Some other works leverage GANs to further boost the visual quality(Lee et al. 2018).

So far, the success of VAE-based video prediction methods has been limited to synthetic videos or scripted videos, such as video games or synthetic shapes rendered with multiple futures(Xue et al. 2016; Babaeizadeh et al. 2017), BAIR robotic pushing dataset(Ebert et al. 2017) with randomly moving robotic arms that conduct multiple possible movements(Babaeizadeh et al. 2017; Lee et al. 2018), or KTH(Schuldt, Laptev, and Caputo 2004) and Human3.6M(Ionescu et al. 2013) where one volunteer repeatedly conducts predefined activities (such as hand clapping and walking) in well controlled environments(Lee et al. 2018; Denton and Fergus 2018; Babaeizadeh et al. 2017; Minderer et al. 2019). In these datasets, multiple futures are created for a given observation, so that the VAE model can be trained as desired. However, videos captured in the wild are usually determinate. There is always a unique future for a given observation. Such a data distribution can easily result in posterior collapse and degenerate VAE to a deterministic model. A possible fix is to treat future frames at multiple time steps as multiple futures at a single time step(Xue et al. 2016; Walker et al. 2016), but such manipulation creates a non-negligible gap between the distributions of the training data and the real-world data. In this paper, we propose VAE² to alleviate the posterior collapse problem in variational video prediction. Different from previous attempts that address model collapse in VAEs such as employing weak decoder(Bowman et al. 2015; Gulrajani et al. 2016), involving stronger constraints(Higgins et al. 2017; Goyal et al. 2017) or annealing strategy(Kim et al. 2018; Gulrajani et al. 2016; Bowman et al. 2015), VAE² is specially designed to handle the collapse problem caused by videos lacking of stochasticity.

VAE-in-VAE

In this section, we elaborate the proposed VAE² step by step. We start with introducing the VAE’s posterior collapse in video prediction caused by the determinate data pair. Next, we describe how to overcome this problem by injecting stochasticity into vanilla VAE’s objective function. Then, we propose a tractable lower bound to facilitate gradient-based solution and finally derive the VAE-in-VAE structure

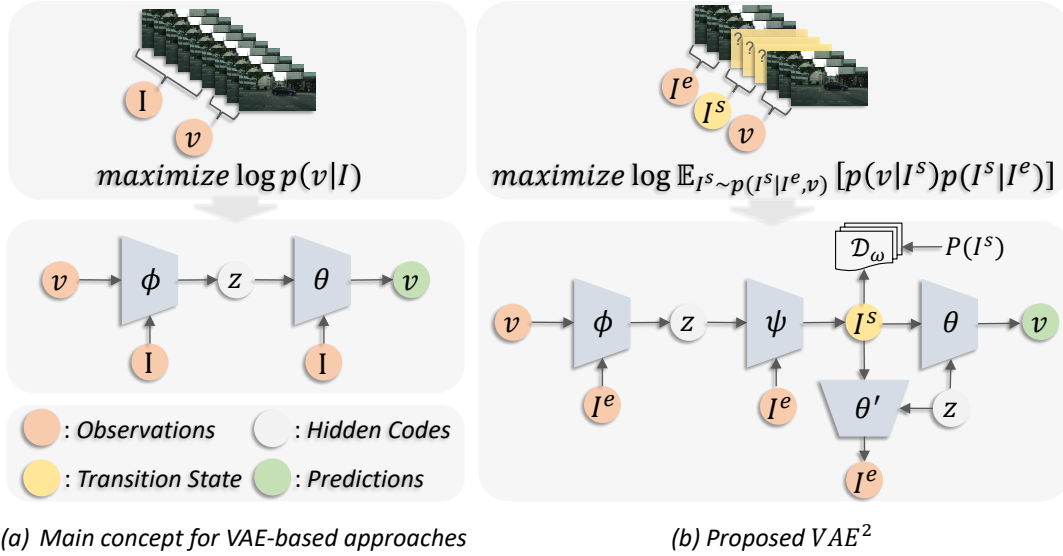


Figure 1: Schematic diagrams of vanilla VAE-based video prediction approach and our VAE² approach. ϕ is the encoder that maps the observation I and future v to a hidden random variable z . θ is the decoder which predicts stochastic future based on the observation and random signal sampled from z . When the future is determinate, the decoder θ can well reconstruct the future without accessing the random hidden code z . As a consequence, it leads VAE to a deterministic model. Unlike vanilla VAE that maximizes the log likelihood of determinate pair (v, I) , we propose to treat part of the observation as an unknown transition state (frames I^s), and maximize the likelihood of the Markov Chain under all possible transition state. Such formulation breaks the direct dependence between future and observation, so that our method models a stochastic process. A nested VAE structure is then derived for end-to-end optimization, where ψ and θ' are two additional decoder to produce the transition frames and reconstruct the observed frames, respectively. D_ω is a discriminator to help generate more realistic transitiona state frames.

for end-to-end optimization.

Posterior Collapse of Vanilla VAE with Determinate Data Pair

We first briefly introduce the formulation of traditional VAE-based solutions for video predictions. Let $\mathcal{D} = \{(I_k, v_k)\}$ denote some i.i.d. data pairs consisting of K samples. Assuming v is conditioned on I with some random processes involving an unobserved hidden variable z , one can maximize the conditional data likelihood $\sum_{k=1}^K \log p(v_k | I_k)$ with conditioned VAEs (c-VAEs) through maximizing the variational lower bound

$$\mathbb{E}_{q_\phi(z_k | I_k, v_k)} [p_\theta(v_k | I_k, z_k)] - KL(q_\phi(z_k | I_k, v_k) || p(z)), \quad (1)$$

where q_ϕ is a parametric model that approximates the true posterior $p(z_k | I_k, v_k)$, p_θ is a generative model w.r.t. the hidden code z_k and the data I_k . KL denotes the Kullback-Leibler(KL) Divergence.

When VAE is used for stochastic video prediction, each $I_k \in \mathbb{R}^{T_I \times H \times W}$ represents an observed video sequence consisting of T_I consecutive frames with $H \times W$ spatial size, $v_k \in \mathbb{R}^{T_v \times H \times W}$ is the future sequence of the observation consisting of T_v consecutive frames. A general framework for variational video prediction is illustrated in Fig. 1 (a), where an encoder ϕ and a decoder θ are employed to instantiate q_ϕ and p_θ , respectively.

In Eq. 1, there is a regression term $p_\theta(v_k | I_k, z_k)$ which

is usually modeled by a deep decoder that takes as inputs the observation I_k and hidden code z_k and directly regresses the future v_k . Since the videos in the wild are determinately captured, each I_k is only associated with a unique v_k without stochasticity. In principle, such determinate data pair (I_k, v_k) can be easily fit by the decoder θ since networks with sufficient capacity are capable of representing arbitrarily complex functions(Hornik et al. 1989) or even memorize samples(Arpit et al. 2017). Therefore, the hidden code z can be entirely ignored by the decoder to fulfill the KL divergence term based on the information preference property(Chen et al. 2016). As a result, VAE is modeling a deterministic process under this scenario.

From VAE to VAE² by Introducing Stochasticity

The reason for the aforementioned collapse issue is that traditional c-VAEs maximize the likelihood $p(v_k | I_k)$ over data pair (v_k, i_k) which has no stochastic behavior. The key to avoid such collapse is to ensure that the VAE is modeling a stochastic process instead of a deterministic one. To achieve this, we split each observation I_k into two parts: determinate observation $I_k^e \in \mathbb{R}^{\frac{T_I}{2} \times H \times W}$ and random transition state $I_k^s \in \mathbb{R}^{\frac{T_I}{2} \times H \times W}$. Different from the determinate I_k^e , I_k^s is treated as a random event that bridges the determinate observation and the unknown future. Assuming that evolution of a video sequence subjects to a Markov process, where the generation process of a sequence is only conditioned on its

previous sequence, we propose to maximize the likelihood of the Markov Chain over observations and futures under all possible transition states. The optimization problem can be expressed as

$$\text{maximize } \log \mathbb{E}_{p(I_k^s | v_k, I_k^e)} [p(v_k | I_k^s) p(I_k^s | I_k^e)]. \quad (2)$$

Intuitively, the proposed objective function involves stochastic information by explicitly relaxing a part of determinate observations to random transition state. However, such formulation is intractable in terms of both the likelihood of the Markov Chain and the expectation term.

A Tractable Objective Function for VAE²

In this section, we demonstrate that a tractable lower bound for Eq. 2 can be derived by applying Cauchy-Schwarz inequality. Specifically, we have

$$\begin{aligned} & \log \mathbb{E}_{p(I^s | v, I^e)} [p(v | I^s) p(I^s | I^e)] \\ & \geq \mathbb{E}_{q_\phi(z | I^e, v)} [\log \mathbb{E}_{p(I^s | I^e, z)} p_\theta(v | I^s, z)] \\ & \quad - KL(q_\phi(z | I^e, v) || p(z)). \end{aligned} \quad (3)$$

Here we omit index k for simplicity. The above lower bound serves as our first-level objective function. It has a similar form as Eq. 1 except that we have one additional transition variable I^s in the decoder model p_θ . To maximize this lower bound, we need to calculate the expectation term $\mathbb{E}_{p(I^s | I^e, z)} p_\theta(v | I^s, z)$ in Eq. 3, which requires an approximation towards $p(I^s | I^e, z)$. Here, we employ a generation model $q_\psi(I^s | I^e, z)$ parameterized with ψ for the approximation by minimizing $KL(q_\psi(I^s | I^e, z) || p(I^s | I^e, z))$, which induces our second-level objective function

$$\mathbb{E}_{q_\psi(I^s | I^e, z)} \log p_{\theta'}(I^e | I^s, z) - KL(q_\psi(I^s | I^e, z) || p(I^s)). \quad (4)$$

For the full derivation of Eq. 3 and Eq. 4, **please refer to our appendix**. Since transition state I^s is high-dimensional signals (video sequences), the exact functional form of its prior distribution is not accessible. We follow adversarial autoencoders (Makhzani et al. 2015) to leverage adversarial training to minimize the distance between the $q_\psi(I^s | I^e, z)$ and the prior $p(I^s)$. As such, $-KL(q_\psi(I^s | I^e, z) || p(I^s))$ in Eq. 4 is replaced by

$$D_\omega(I^s, I_{prior}), \text{ where } I_{prior} \sim p(I^s), I^s \sim q_\psi(I^s | I^e, z). \quad (5)$$

Here, D_ω is a discriminator network parameterized with ω and I_{prior} is randomly sampled from the video dataset. By doing so, the second-level objective function Eq. 4 is now tractable. Ideally, we shall optimize the first-level and second-level objective function iteratively, which requires unaffordable training time for convergence. In practice, we simplify such iterative learning process by merging the two objective functions into a single one as

$$\begin{aligned} & \mathcal{L}(I^e, I^s, v; \theta, \phi) + \\ & \lambda [\mathbb{E}_{q_\psi(I^s | I^e, z)} \log p_{\theta'}(I^e | I^s, z) + D_\omega(I^s, I_{prior})], \end{aligned} \quad (6)$$

where λ is a loss weight applied on Eq. 4. This simplification enables us to simultaneously optimize the two objective functions and we use a weight λ to adjust the optimization speed of our second-level objective function to mimic the original iterative process.

End-to-end Optimization

We employ two VAE structures to maximize our final objective function in Eq. 6. As illustrated in Fig. 1(b), the first VAE consisting of an encoder ϕ and a decoder θ is incorporated to maximize the first-level objective function $\mathcal{L}(I^e, I^s, v; \theta, \phi)$. The second VAE with an encoder ψ , a decoder θ' and a discriminator D_ω is used for maximizing the second-level objective function. We assume p_θ and $p_{\theta'}$ to be Laplace distribution (which leads to L1 regression loss) and assume q_ϕ to be Gaussian. The training procedure can be summarized as follows:

- Encoder ϕ takes I^e and v as inputs and produces hidden codes z . z is fed into ψ to generate L different I^s . For each I^s , decoder θ and θ' reconstruct v and I^e , respectively.
- Estimate the $\log \mathbb{E}_{p(I^s | I^e, z)} p_\theta(v | I^s, z)$ in Eq. 3 with $\log \sum_{i=1}^L p_\theta(v | I_i^s, z)$. Estimate $\mathbb{E}_{q_\psi(I^s | I^e, z)} \log p_{\theta'}(I^e | I^s, z)$ in Eq. 6 with $\sum_{i=1}^L \log p_{\theta'}(I^e | I_i^s, z)$.
- Compute gradients w.r.t. Eq. 6 and update $\phi, \psi, \theta, \theta'$. Update D_ω with adversarial learning.

In practice, we observe that this simplified process works well even with $L = 1$. This further reduces the algorithm complexity.

Number Sequence Prediction

We first use a simple number sequence prediction task to demonstrate how VAE² mitigates the collapse problem when only determinate data are available. More specifically, we explicitly design a world model which can stochastically produce number sequences w.r.t. the given model parameter.

Sequence Model Design. The stochastic model that generates number sequence is defined by $G(\alpha, H(\epsilon)) = \frac{1}{1 + e^{-\alpha H(\epsilon)}}$. Here, $H(\epsilon) = [h_0(\epsilon_0), h_1(\epsilon_1), \dots, h_{N-1}(\epsilon_{N-1})] \in \mathbb{R}^N$ and $h_i(\epsilon_i) = C + i * S + \epsilon_i$, where $\epsilon_i \sim \text{Uniform}(0, S)$. This world model is parameterized by α and its stochastic nature is characterized by $H(\epsilon)$.

Constructing the Dataset. In order to mimic the determinate video sequences captured in the wild, we use $G(\alpha, H(\epsilon))$ to generate only one number sequence for each world parameter α . We then split each number sequence into three even parts. For VAE², the three parts correspond to I^e , I^s and v , respectively. For the baseline VAE, the first and the second parts together correspond to I and the third part corresponds to v . The dataset $D = \{G(\alpha_k, H(\hat{\epsilon})), k \in [1, K]\}$ contains K number sequences generated from K different world model parameters, where $H(\hat{\epsilon})$ denotes a single sampling result of $H(\epsilon)$. We set C, S, N , and K to -1.5, 0.1, 30 and 10,000, respectively. The constructed dataset contains 10,000 number sequences, each of which has 30 data points.

Evaluation and Visualization. We train our VAE², VAE (Babaeizadeh et al. 2017) and VAE-GAN (Lee et al. 2018) models on this number sequence dataset, respectively. The training and architecture details can be found in the appendix. After training, we make 100 predictions on v using each method. In Fig. 2, we plot original data points in red

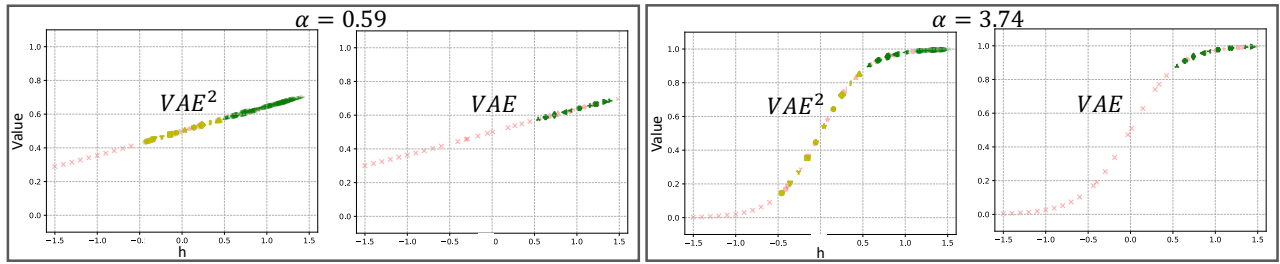


Figure 2: Visualization of the number sequence prediction at two model parameters. The 100 predictions made by VAE baseline are almost identical while those made by the proposed VAE² are more scattered around the groundtruth. This shows that VAE² captures the inherent stochastic law of the number sequences model.

and predicted ones in green. The different shapes correspond to different hidden variables $h_i(\epsilon_i)$.

We observe from the figure that the predicted v from the baseline VAE model are almost identical among the 100 predictions (samples of the same shape are grouped together), showing that the baseline VAE degrades to a deterministic model. In contrast, the proposed VAE² provides much more diverse predictions (samples of each shape scatter around the ground-truth). Although we do not provide multiple futures in the training dataset, VAE² is able to explore the underlying stochastic information through our innovative design. More visualizations can be found in the appendix.

In addition to visualizing the predicted numbers, we can use the standard deviation of the L1 loss of different samples to measure the diversity of predictions. Fig. 3(a) plots the mean and the standard deviation of the predictions from VAE² and its counterparts on the entire dataset. It is clear that the number sequences predicted by the proposed VAE² are more diverse than other methods.

Experiments on Videos Captured in the Wild

Dataset and Evaluation Metrics. We evaluate the proposed VAE² with the Cityscapes dataset (Cordts et al. 2016) which contains urban street scenes from 50 different cities. The videos are captured at 17 fps with cameras mounted on moving cars. Since a car and its mounted camera pass each street only once, every video sequence is determinate and there are no multiple futures available. The average number of humans and vehicles per frame is 7.0 and 11.8, respectively, providing a fairly complex instance pattern.

There is no consensus yet on how to evaluate a video prediction scheme. Previous work has tried to evaluate the perceived visual quality of the predicted frames. However, this work is focused on mitigating the model collapse problem caused by determinate training data. In addition to the perceived visual quality, we will mainly evaluate how seriously a prediction model suffers from the model collapse problem. In general, the more diverse the predicted frames are, the better the model handles the model collapse problem. The diversity of predicted frames can be evaluated both quantitatively and qualitatively. In particular, we use the standard deviation of some conventional image quality evaluation metrics, such as SSIM (Wang et al. 2004), PSNR (Huynh-Thu and Ghanbari 2008), and L1 loss, for quantitative evalua-

tion. We also compute the optical flows between the ground-truth future frame and the predicted future frames by various prediction models. Since optical flow reflects per-pixel displacement, it can be a very intuitive way to show the pixel-level difference between the two frames.

Reference Schemes and Implementation Details. Existing VAE-based video prediction approaches are designed with different backbone networks and data structures, including RGB frames, skeleton, or dense trajectory. In this work, we only consider methods that directly operate on raw RGB videos to demonstrate the efficacy of the proposed VAE². These prediction models can be categorized into two VAE variants, namely vanilla VAEs (Babaeizadeh et al. 2017; Xue et al. 2016; Denton and Fergus 2018) and VAE-GAN (Lee et al. 2018; Larsen et al. 2015). In addition, we evaluate β -VAE (Higgins et al. 2017) and VAE with annealing (Bowman et al. 2015) which are designed for addressing the model collapse problem without considering the situation where training data lack of stochasticity. We also construct a deterministic model as a baseline.

We employ 18-layer HRNet (wd-18-small) (Sun et al. 2019) to instantiate all the encoders, decoders, and GANs in VAE². For fair comparison, we replace the original backbone network in the reference schemes (Babaeizadeh et al. 2017; Lee et al. 2018; Higgins et al. 2017; Bowman et al. 2015) with the same HRNet. The deterministic baseline is also a 18-layer HRNet which directly regresses the future frames. We set λ to 0.1 and we use Adam optimizer to train all methods for 1,000 epochs. More training details can be found in the appendix.

Diversity and Quality. In order to measure the diversity of the predictions, we make 100 random predictions with each method and compute the PSNR, L1 distance, SSIM, and multi-scale SSIM (MS-SSIM) (Wang, Simoncelli, and Bovik 2003) between each predicted frame and the ground-truth future frame. In Fig. 3, we use box-and-whisker charts to plot the mean (the center of each box), the 3-sigma (solid box), and the 5-sigma (whiskers) of each metric, where sigma denotes the standard deviation. In each sub-figure, different colors represent different methods. It is clear from the figure that the future frames predicted by VAE² have a larger standard deviation than the reference schemes. It corroborates that VAE² can predict much more diverse futures than existing methods. Besides, we can find that approaches such

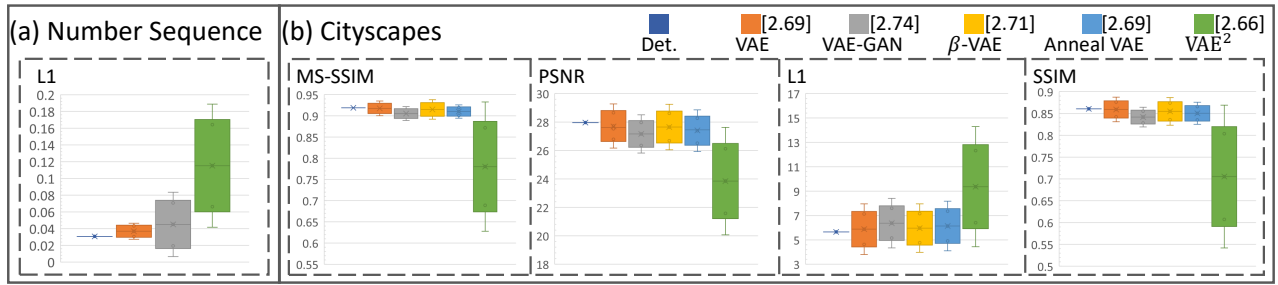


Figure 3: Standard deviation of 100 prediction samples from different methods under four criteria. Each box and whisker indicates the mean \pm three times and five times standard deviation, respectively. Larger deviation range of VAE² indicates it can significantly improve the diversity of the predictions. The number beside each legend denotes the averaged Inception Score of the 100 samples from corresponding method over the entire Cityscapes dataset.

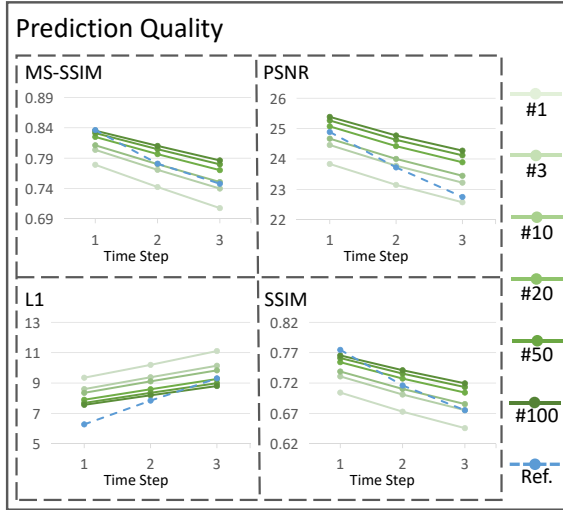


Figure 4: Prediction qualities under different numbers of samples. VAE² can generate predictions very close to the ground truth future when it is sampled for sufficient times.

as β -VAE and Anneal-VAE that are designed for model collapse fail in this scenario. They only bring marginal diversity improvement. This implies that we need a specific solution like VAE² when source data lack stochasticity.

Another intuitive way to check whether the proposed VAE² helps alleviate the model collapse problem is to evaluate the KL loss of the hidden code z . A variational model that collapses to its deterministic counterpart usually has a very small KL loss. As can be viewed in Fig. 5, the converged KL loss of counterpart methods is significantly smaller than that of VAE².

Finally, we follow the methods in (Babaeizadeh et al. 2017) to evaluate the video prediction quality. In Fig. 4, we plot the best prediction among different numbers of samples under various metrics. The reference is a deterministic model (Finn, Goodfellow, and Levine 2016) that directly regresses the ground-truth future. We can see from the figure that as the number of samples increases, the proposed VAE² can predict video sequences at a quality that is comparable

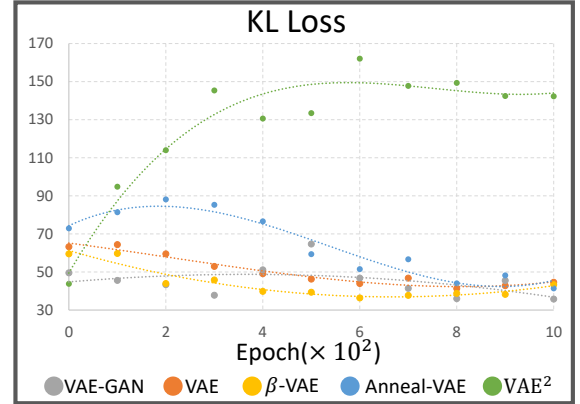


Figure 5: KL loss (without normalization) of the latent variable z during training for different schemes. Small KL loss indicates the learned distribution of the hidden variable z is very close to the prior distribution. When KL loss approaches to zero, the latent variable does not encode any useful information.

with the reference model in terms of the reconstruction fidelity. As the time-step increases, VAE² achieves an even better performance than the reference. We also employ Inception Score (IS) (Salimans et al. 2016), a frequently used no-reference image quality assessment method, to measure the visual quality of the predicted futures. As illustrated by the number beside each legend in Fig. 3, the scores are close to each other, which suggests the overall visual quality of the futures predicted by VAE² are on par with other approaches.

Visualizations. Due to limited space, we only visualize single frame predictions with three baseline methods in this section. More visualizations can be found in the appendix. Fig. 7 shows three sampled predictions of a single prediction step for each of the schemes to be compared. We notice that the future positions of the fast moving truck predicted by VAE (Babaeizadeh et al. 2017) and VAE-GAN (Lee et al. 2018) are almost identical to the deterministic baseline. There is little stochasticity among different samples. In contrast, VAE² achieves noticeable randomness on the moving truck and the moving camera. The predicted camera motion























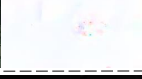


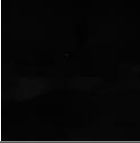




	Det.	VAE		VAE-GAN		VAE ²
Samples & Flows						
						
						
						
Flow Variance						
Method	Det.	VAE	VAE-GAN	β -VAE	Anneal-VAE	VAE ²
Flow Std.	0.0	1.9697	2.6049	1.7984	2.1413	11.2991

Figure 6: Visualization of predictions and their corresponding optical flow w.r.t. the ground-truth future. We randomly sample four futures with each method. The diverse patterns of the flow images under VAE² indicate its stochastic behavior. The last row shows the standard deviations of the flow images over 100 samples. The large value of VAE² supports that it predicts much more diverse future. More visualizations can be found in the appendix.

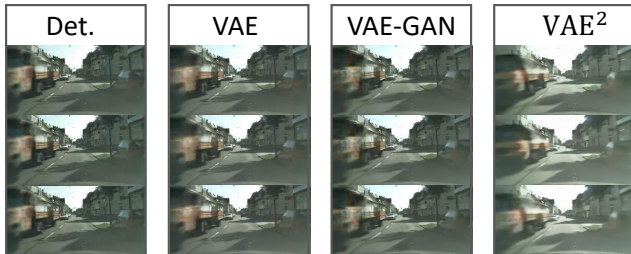


Figure 7: Visualization of three predictions for the next frame of an observed video sequence. Each column contains the three predictions made by each method. It can be observed that VAE² predicts quite different futures while the others make almost identical predictions.

can be observed from the parking car on the right.

In order to show the detailed difference among predictions, we compute and colorize (Baker et al. 2011) the optical flow between each prediction and the ground-truth future frame. In Fig. 6, we show four predictions of each method and their corresponding optical flow. The color code for optical flows is illustrated at the top-left corner. For example, the first flow map under VAE² has a green hue, suggesting that the whole background shifts left w.r.t. the ground truth future. This means the camera car is predicted to turn right in the coming future (although it is not the ground-truth future in the dataset). It can also be observed that the displacement patterns of the frames predicted by our method are much more diverse than the other approaches. To quantify such

diversity, we compute and visualize the (normalized) standard deviation of the optical flows on 100 different samples for each method. As can be viewed in fifth row, the flow variance of VAE² has much larger responses on the moving car and the whole background region. The statistics of such diversity on the entire dataset are presented in the table at the last row to illustrate the efficacy of VAE² on predicting stochastic futures.

Conclusion and Discussion

In this paper, we investigate the posterior collapse problem in variational video prediction caused by the videos determinately captured in the wild. We effectively mitigate this problem by explicitly introducing stochasticity into vanilla VAEs and propose an end-to-end framework, VAE², for optimization. The proposed VAE² demonstrates its capability of capturing the stochastic information of videos in the wild, which makes variational video prediction more practical in real-world applications. In addition, we believe that VAE² can be effectively extended to other sequential prediction problems where training data are lack of stochasticity. We will leave this part to future works.

We also notice that the inference structure of VAE² looks similar to the recently proposed two-stage VAE (Dai and Wipf 2019). However, this two-stage VAE is designed to address the problem that the hidden code drawn from the encoder is incongruous with the prior, and the first VAE is used to predict the distribution of the hidden code instead of the randomized partial observation as in VAE².

References

- Alemi, A. A.; Poole, B.; Fischer, I.; Dillon, J. V.; Saurous, R. A.; and Murphy, K. 2017. Fixing a broken ELBO. *arXiv preprint arXiv:1711.00464*.
- Arpit, D.; Jastrzebski, S.; Ballas, N.; Krueger, D.; Bengio, E.; Kanwal, M. S.; Maharaj, T.; Fischer, A.; Courville, A.; Bengio, Y.; et al. 2017. A closer look at memorization in deep networks. *arXiv preprint arXiv:1706.05394*.
- Babaeizadeh, M.; Finn, C.; Erhan, D.; Campbell, R. H.; and Levine, S. 2017. Stochastic variational video prediction. *arXiv preprint arXiv:1710.11252*.
- Baker, S.; Scharstein, D.; Lewis, J.; Roth, S.; Black, M. J.; and Szeliski, R. 2011. A database and evaluation methodology for optical flow. *International journal of computer vision* 92(1): 1–31.
- Bowman, S. R.; Vilnis, L.; Vinyals, O.; Dai, A. M.; Jozefowicz, R.; and Bengio, S. 2015. Generating sentences from a continuous space. *arXiv preprint arXiv:1511.06349*.
- Chen, X.; Kingma, D. P.; Salimans, T.; Duan, Y.; Dhariwal, P.; Schulman, J.; Sutskever, I.; and Abbeel, P. 2016. Variational lossy autoencoder. *arXiv preprint arXiv:1611.02731*.
- Cordts, M.; Omran, M.; Ramos, S.; Rehfeld, T.; Enzweiler, M.; Benenson, R.; Franke, U.; Roth, S.; and Schiele, B. 2016. The cityscapes dataset for semantic urban scene understanding. In *Proceedings of the IEEE conference on computer vision and pattern recognition*, 3213–3223.
- Dai, B.; and Wipf, D. 2019. Diagnosing and enhancing vae models. *arXiv preprint arXiv:1903.05789*.
- Denton, E.; and Fergus, R. 2018. Stochastic video generation with a learned prior. *arXiv preprint arXiv:1802.07687*.
- Ebert, F.; Finn, C.; Lee, A. X.; and Levine, S. 2017. Self-supervised visual planning with temporal skip connections. *arXiv preprint arXiv:1710.05268*.
- Finn, C.; Goodfellow, I.; and Levine, S. 2016. Unsupervised learning for physical interaction through video prediction. In *Advances in neural information processing systems*, 64–72.
- Goodfellow, I.; Pouget-Abadie, J.; Mirza, M.; Xu, B.; Warde-Farley, D.; Ozair, S.; Courville, A.; and Bengio, Y. 2014. Generative adversarial nets. In *Advances in neural information processing systems*, 2672–2680.
- Goyal, A. G. A. P.; Sordoni, A.; Côté, M.-A.; Ke, N. R.; and Bengio, Y. 2017. Z-forcing: Training stochastic recurrent networks. In *Advances in neural information processing systems*, 6713–6723.
- Gulrajani, I.; Kumar, K.; Ahmed, F.; Taiga, A. A.; Visin, F.; Vazquez, D.; and Courville, A. 2016. Pixelvae: A latent variable model for natural images. *arXiv preprint arXiv:1611.05013*.
- Guo, Q.; Feng, W.; Zhou, C.; Huang, R.; Wan, L.; and Wang, S. 2017. Learning dynamic siamese network for visual object tracking. In *Proceedings of the IEEE International Conference on Computer Vision*, 1763–1771.
- Higgins, I.; Matthey, L.; Pal, A.; Burgess, C.; Glorot, X.; Botvinick, M.; Mohamed, S.; and Lerchner, A. 2017. beta-VAE: Learning Basic Visual Concepts with a Constrained Variational Framework. *Iclr* 2(5): 6.
- Hochreiter, S.; and Schmidhuber, J. 1997. Long short-term memory. *Neural computation* 9(8): 1735–1780.
- Hornik, K.; Stinchcombe, M.; White, H.; et al. 1989. Multilayer feedforward networks are universal approximators. *Neural networks* 2(5): 359–366.
- Huynh-Thu, Q.; and Ghanbari, M. 2008. Scope of validity of PSNR in image/video quality assessment. *Electronics letters* 44(13): 800–801.
- Ionescu, C.; Papava, D.; Olaru, V.; and Sminchisescu, C. 2013. Human3.6m: Large scale datasets and predictive methods for 3d human sensing in natural environments. *IEEE transactions on pattern analysis and machine intelligence* 36(7): 1325–1339.
- Jia, X.; De Brabandere, B.; Tuytelaars, T.; and Gool, L. V. 2016. Dynamic filter networks. In *Advances in Neural Information Processing Systems*, 667–675.
- Kalchbrenner, N.; van den Oord, A.; Simonyan, K.; Danihelka, I.; Vinyals, O.; Graves, A.; and Kavukcuoglu, K. 2017. Video pixel networks. In *Proceedings of the 34th International Conference on Machine Learning-Volume 70*, 1771–1779. JMLR. org.
- Kim, Y.; Wiseman, S.; Miller, A. C.; Sontag, D.; and Rush, A. M. 2018. Semi-amortized variational autoencoders. *arXiv preprint arXiv:1802.02550*.
- Kingma, D. P.; and Welling, M. 2013. Auto-encoding variational bayes. *arXiv preprint arXiv:1312.6114*.
- Larsen, A. B. L.; Sønderby, S. K.; Larochelle, H.; and Winther, O. 2015. Autoencoding beyond pixels using a learned similarity metric. *arXiv preprint arXiv:1512.09300*.
- Lee, A. X.; Zhang, R.; Ebert, F.; Abbeel, P.; Finn, C.; and Levine, S. 2018. Stochastic adversarial video prediction. *arXiv preprint arXiv:1804.01523*.
- Liu, Z.; Yeh, R. A.; Tang, X.; Liu, Y.; and Agarwala, A. 2017. Video frame synthesis using deep voxel flow. In *Proceedings of the IEEE International Conference on Computer Vision*, 4463–4471.
- Lu, C.; Hirsch, M.; and Scholkopf, B. 2017. Flexible spatio-temporal networks for video prediction. In *Proceedings of the IEEE Conference on Computer Vision and Pattern Recognition*, 6523–6531.
- Makhzani, A.; Shlens, J.; Jaitly, N.; Goodfellow, I.; and Frey, B. 2015. Adversarial autoencoders. *arXiv preprint arXiv:1511.05644*.
- Minderer, M.; Sun, C.; Villegas, R.; Cole, F.; Murphy, K. P.; and Lee, H. 2019. Unsupervised learning of object structure and dynamics from videos. In *Advances in Neural Information Processing Systems*, 92–102.
- Mirza, M.; and Osindero, S. 2014. Conditional generative adversarial nets. *arXiv preprint arXiv:1411.1784*.

- Oh, J.; Guo, X.; Lee, H.; Lewis, R. L.; and Singh, S. 2015. Action-conditional video prediction using deep networks in atari games. In *Advances in neural information processing systems*, 2863–2871.
- Oord, A. v. d.; Kalchbrenner, N.; and Kavukcuoglu, K. 2016. Pixel recurrent neural networks. *arXiv preprint arXiv:1601.06759*.
- Ranzato, M.; Szlam, A.; Bruna, J.; Mathieu, M.; Collobert, R.; and Chopra, S. 2014. Video (language) modeling: a baseline for generative models of natural videos. *arXiv preprint arXiv:1412.6604*.
- Razavi, A.; Oord, A. v. d.; Poole, B.; and Vinyals, O. 2019. Preventing posterior collapse with delta-vaes. *arXiv preprint arXiv:1901.03416*.
- Salimans, T.; Goodfellow, I.; Zaremba, W.; Cheung, V.; Radford, A.; and Chen, X. 2016. Improved techniques for training gans. In *Advances in neural information processing systems*, 2234–2242.
- Schuldt, C.; Laptev, I.; and Caputo, B. 2004. Recognizing human actions: a local SVM approach. In *Proceedings of the 17th International Conference on Pattern Recognition, 2004. ICPR 2004.*, volume 3, 32–36. IEEE.
- Srivastava, N.; Mansimov, E.; and Salakhudinov, R. 2015. Unsupervised learning of video representations using lstms. In *International conference on machine learning*, 843–852.
- Sun, K.; Xiao, B.; Liu, D.; and Wang, J. 2019. Deep high-resolution representation learning for human pose estimation. In *Proceedings of the IEEE Conference on Computer Vision and Pattern Recognition*, 5693–5703.
- Thrun, S.; Montemerlo, M.; Dahlkamp, H.; Stavens, D.; Aron, A.; Diebel, J.; Fong, P.; Gale, J.; Halpenny, M.; Hoffmann, G.; et al. 2006. Stanley: The robot that won the DARPA Grand Challenge. *Journal of field Robotics* 23(9): 661–692.
- Villegas, R.; Yang, J.; Hong, S.; Lin, X.; and Lee, H. 2017. Decomposing motion and content for natural video sequence prediction. *arXiv preprint arXiv:1706.08033*.
- Vondrick, C.; Pirsivash, H.; and Torralba, A. 2016. Generating videos with scene dynamics. In *Advances in neural information processing systems*, 613–621.
- Vondrick, C.; and Torralba, A. 2017. Generating the future with adversarial transformers. In *Proceedings of the IEEE Conference on Computer Vision and Pattern Recognition*, 1020–1028.
- Walker, J.; Doersch, C.; Gupta, A.; and Hebert, M. 2016. An uncertain future: Forecasting from static images using variational autoencoders. In *European Conference on Computer Vision*, 835–851. Springer.
- Walker, J.; Gupta, A.; and Hebert, M. 2015. Dense optical flow prediction from a static image. In *Proceedings of the IEEE International Conference on Computer Vision*, 2443–2451.
- Wang, Z.; Bovik, A. C.; Sheikh, H. R.; and Simoncelli, E. P. 2004. Image quality assessment: from error visibility to structural similarity. *IEEE transactions on image processing* 13(4): 600–612.
- Wang, Z.; Simoncelli, E. P.; and Bovik, A. C. 2003. Multi-scale structural similarity for image quality assessment. In *The Thrity-Seventh Asilomar Conference on Signals, Systems & Computers, 2003*, volume 2, 1398–1402. Ieee.
- Wichers, N.; Villegas, R.; Erhan, D.; and Lee, H. 2018. Hierarchical long-term video prediction without supervision. *arXiv preprint arXiv:1806.04768*.
- Xue, T.; Wu, J.; Bouman, K.; and Freeman, B. 2016. Visual dynamics: Probabilistic future frame synthesis via cross convolutional networks. In *Advances in neural information processing systems*, 91–99.
- Zhou, Y.; Sun, X.; Zha, Z.-J.; and Zeng, W. 2018. Mict: Mixed 3d/2d convolutional tube for human action recognition. In *Proceedings of the IEEE conference on computer vision and pattern recognition*, 449–458.

VAE²: Appendix

Anonymous Author(s)

Affiliation

Address

email

1 This appendix provides the following information, which is not included in the submitted paper due
2 to space limitation.

- 3 - The detailed proof of eq. (3) and eq. (4) in the paper
- 4 - Analysis on the tightness of the lower bound.
- 5 - More details on experimental setup and parameter tuning.
- 6 - More visualizations.

7 In order to better present the equations involved in our paper, we employ a single-column format for
8 this appendix material.

9 1 A Tractable Objective Function

10 1.1 Proof of eq. (3) in the paper

11 Assuming that the evolution of a video sequence subjects to a Markov process, where the generation
12 process of a sequence is only conditioned on its previous sequence, we have

$$\begin{aligned}
 & \log \mathbb{E}_{p(I^s|v, I^e)}[p(v | I^s)p(I^s | I^e)] \\
 &= \log \mathbb{E}_{p(I^s|v, I^e)}[p(v | I^s, I^e)p(I^s | I^e)] \\
 &= \log \mathbb{E}_{p(I^s|v, I^e)}[p(v, I^s | I^e)] \\
 &= \log \sum_{I^s} p(v, I^s | I^e)p(I^s | v, I^e) \\
 &= \log \frac{\sum_{I^s} p(v, I^s | I^e)p(v, I^s | I^e)}{p(v | I^e)}.
 \end{aligned} \tag{1}$$

13 The Cauchy–Schwarz inequality states that for vectors u and v in an inner product space, it is true
14 that $|\langle u, v \rangle|^2 \leq \langle u, u \rangle \cdot \langle v, v \rangle$, where $\langle \cdot, \cdot \rangle$ is the inner product. Based on this inequality, we have

$$\log \frac{\sum_{I^s} p(v, I^s | I^e)p(v, I^s | I^e)}{p(v | I^e)} \geq \log \frac{\frac{1}{C}[\sum_{I^s} p(v, I^s | I^e)]^2}{p(v | I^e)} = \log p(v | I^e) - \log C, \tag{2}$$

15 where C is a constant. Note that a trivial solution here is to directly employ a vanilla c-VAE to
16 maximize the lower bound $\log p(v | I^e)$. However, it is still based on the determinate data pair
17 (I^e, v) . By bringing back I^s , we derive a non-trivial solution as follows. Let $q_\phi(z | I^e, v)$ denote
18 a variational distribution that approximates the true posterior $p(z | I^e, v)$ and assuming that the

19 likelihood $p(v \mid I^s, z)$ comes from parametric families of distribution $p_\theta(v \mid I^s, z)$, we have

$$\begin{aligned}
& \log p(v \mid I^e) \\
&= \mathbb{E}_{q_\phi(z \mid I^e, v)} [\log p(v \mid I^e)] \\
&= \mathbb{E}_{q_\phi(z \mid I^e, v)} \left[\log \frac{p(z)p(v \mid I^e, z)}{p(z \mid I^e, v)} \right] \\
&= \mathbb{E}_{q_\phi(z \mid I^e, v)} \left[\log \frac{p(z)p(v \mid I^e, z)q_\phi(z \mid I^e, v)}{p(z \mid I^e, v)q_\phi(z \mid I^e, v)} \right] \\
&= \mathbb{E}_{q_\phi(z \mid I^e, v)} [\log p(v \mid I^e, z)] + \mathbb{E}_{q_\phi(z \mid I^e, v)} \left[\log \frac{p(z)}{q_\phi(z \mid I^e, v)} \right] + \mathbb{E}_{q_\phi(z \mid I^e, v)} \left[\log \frac{q_\phi(z \mid I^e, v)}{p(z \mid I^e, v)} \right] \\
&= \mathbb{E}_{q_\phi(z \mid I^e, v)} \left[\log \sum_{I^s} p(v, I^s \mid I^e, z) \right] - D_{KL}(q_\phi(z \mid I^e, v) \parallel p(z)) \\
&\quad + D_{KL}(q_\phi(z \mid I^e, v) \parallel p(z \mid I^e, v)) \\
&\geq \mathbb{E}_{q_\phi(z \mid I^e, v)} \left[\log \sum_{I^s} p(v, I^s \mid I^e, z) \right] - D_{KL}(q_\phi(z \mid I^e, v) \parallel p(z)) \\
&= \mathbb{E}_{q_\phi(z \mid I^e, v)} \left[\log \sum_{I^s} p(v, I^s, z)p(I^s \mid I^e, z) \right] - D_{KL}(q_\phi(z \mid I^e, v) \parallel p(z)) \\
&= \mathbb{E}_{q_\phi(z \mid I^e, v)} [\log \mathbb{E}_{p(I^s \mid I^e, z)} p_\theta(v, I^s, z)] - D_{KL}(q_\phi(z \mid I^e, v) \parallel p(z)).
\end{aligned} \tag{3}$$

20 Here D_{KL} denotes the KL divergence and $p(z)$ is the prior distribution of the hidden code z . When
21 assuming $p(z)$ to be a centered isotropic multivariate Gaussian $\mathcal{N}(z; \mathbf{0}, \mathbf{I})$, where \mathbf{I} denotes the
22 identity covariance matrix, $D_{KL}(q_\phi(z \mid I^e, v) \parallel p(z))$ has an analytic form (Please see [1] for more
23 details).

24 1.2 Proof of eq. (4) in the paper

25 Given a specific hidden random variable z sampled with $q_\phi(z \mid I^e, v)$ in the previous step, let
26 $q_\psi(I^s \mid I^e, z)$ denote a variational distribution that approximates the true posterior $p(I^s \mid I^e, z)$
27 and assuming that the likelihood $p(I^e \mid I^s, z)$ comes from parametric families of distribution
28 $p_{\theta'}(I^e \mid I^s, z)$. In addition, we follow the assumption in [1] that the generation of data (video
29 sequence in our case) is a random process involving an unobserved random variable, which can be
30 described with $p(I^e) = \int_z p(I^e \mid z)p(z)$. We rewrite $D_{KL}(q_\psi(I^s \mid I^e, z) \parallel p(I^s \mid I^e, z))$ as

$$\begin{aligned}
& D_{KL}(q_\psi(I^s \mid I^e, z) \parallel p(I^s \mid I^e, z)) \\
&= \mathbb{E}_{q_\psi(I^s \mid I^e, z)} \left[\log \frac{q_\psi(I^s \mid I^e, z)}{p(I^s \mid I^e, z)} \right] \\
&= \mathbb{E}_{q_\psi(I^s \mid I^e, z)} \left[\log \frac{q_\psi(I^s \mid I^e, z)}{p(I^s \mid I^e, z)} + \log \frac{p(I^s)p(I^e \mid I^s, z)}{q_\psi(I^s \mid I^e, z)} - \log \frac{p(I^s)p(I^e \mid I^s, z)}{q_\psi(I^s \mid I^e, z)} \right] \\
&= \mathbb{E}_{q_\psi(I^s \mid I^e, z)} \left[\log \frac{p(I^s)p(I^e \mid I^s, z)}{p(I^s \mid I^e, z)} \right] - \mathbb{E}_{q_\psi(I^s \mid I^e, z)} \left[\log \frac{p(I^s)p(I^e \mid I^s, z)}{q_\psi(I^s \mid I^e, z)} \right] \\
&= \mathbb{E}_{q_\psi(I^s \mid I^e, z)} [\log p(I^e \mid z)] - [\mathbb{E}_{q_\psi(I^s \mid I^e, z)} [\log p(I^e \mid I^s, z)] - D_{KL}(q_\psi(I^s \mid I^e, z) \parallel p(I^s))] \\
&= p(I^e \mid z) - [\mathbb{E}_{q_\psi(I^s \mid I^e, z)} [\log p_{\theta'}(I^e \mid I^s, z)] - D_{KL}(q_\psi(I^s \mid I^e, z) \parallel p(I^s))],
\end{aligned} \tag{4}$$

31 where $p(I^e \mid z)$ is the generation process of the video sequence given a specific z , which can be
32 regarded as an unknown constant here. Thus, minimizing $D_{KL}(q_\psi(I^s \mid I^e, z) \parallel p(I^s \mid I^e, z))$ is
33 equivalent to maximizing $\mathbb{E}_{q_\psi(I^s \mid I^e, z)} [\log p_{\theta'}(I^e \mid I^s, z)] - D_{KL}(q_\psi(I^s \mid I^e, z) \parallel p(I^s))$, which
34 leads to . (4) in the paper.

35 1.3 Tightness Analysis

36 As can be viewed from the Section 1.1 and 1.2 in this appendix, there are two relaxations before
37 we derive the tractable objective function. The first relaxation happens in Eq. (2) which is a stan-
38 dard Cauchy–Schwarz inequality. So its tightness ϵ is the same as that of the Cauchy–Schwarz

inequality. More specifically, we use the difference between the original objective function
 $\log \frac{\sum_{I^s} p(v, I^s | I^e) p(v, I^s | I^e)}{p(v | I^e)}$ and its lower bound $\log \frac{\frac{1}{C} [\sum_{I^s} p(v, I^s | I^e)]^2}{p(v | I^e)}$ to measure ϵ as follows:

$$\begin{aligned} \epsilon &= \log \frac{\sum_{I^s} p(v, I^s | I^e) p(v, I^s | I^e)}{p(v | I^e)} - \log \frac{\frac{1}{C} [\sum_{I^s} p(v, I^s | I^e)]^2}{p(v | I^e)} \\ &= \log \frac{C \sum_{I^s} p(v, I^s | I^e) p(v, I^s | I^e)}{p^2(v | I^e)} \\ &\leq \log \frac{C (\sum_{I^s} p(v, I^s | I^e))^2}{p^2(v | I^e)} = \log C. \end{aligned} \quad (5)$$

As can be viewed here the margin between the original objective function and its lower bound is no greater than a constant $\log C$.

The second relaxation happens in Eq. (3) in the appendix. It is a common variational lower bound and its tightness can be directly obtained from the Eq. (3) which is $D_{KL}(q_\phi(z | I^e, v) || p(z | I^e, v))$.

2 Experimental Setups

2.1 Number Sequence Prediction

Backbone Implementations. We employ a multi-layer perceptron (MLP) with two hidden layers to instantiate all the necessary encoders and decoders in VAE², VAE, VAE-GAN, and the deterministic model. The dimensions of the two hidden layers are both 128. We append a non-linear operation ReLU[2] after each hidden layer.

World Model Parameter α . Parameter α_k used to construct the dataset $D = \{G(\alpha_k, H(\hat{\epsilon})), k \in [1, K]\}$ is defined by $\alpha_k = 0.1 + 0.0005 * (k - 1)$. When K is set to 10,000, α_k ranges from 0.1 to 5.9995. We randomly select 9,000 α_k 's for training and the rest 1,000 are for testing.

Training Details. we use Adam optimizer to train all methods for 1,000 epochs. The weight decay is set to $1e^{-4}$ and the initial learning rate is $1e^{-3}$. The λ is set to 0.02.

2.2 Cityscapes

Backbone Implementations. As discussed in the paper, we employ 18-layer HRNet[3] as the backbone network for every encoder, decoder, and discriminator in all methods for fair comparison. HRNet is initially designed for human pose detection and has been successfully extended to many other fields recently [4]. HRNet is well-known for its preservation of spatial resolution during inference, which is very beneficial to dense prediction tasks such as semantic segmentation and video prediction. The detailed architecture of the HRNet we used in our paper can be found in [4] (referred as HRNetV2-W18).

Similar to ResNet[5], HRNetV2-W18 has a total of four stages. In this paper, for every encoder and decoder which takes the hidden code z as one of the inputs, we concatenate the hidden code to the video sequence's feature maps at the third stage and feed them together into the fourth stage to generate the output. The dimension of the feature maps from the third stage of HRNetV2-W18 is $72 \times 128 \times 256$ (*channel* \times *height* \times *width*) and the dimension of the hidden code z is designed to be $64 \times 1 \times 1$ for all methods in the paper. Therefore we broadcast (repeat) z to a $64 \times 128 \times 256$ map for the concatenation.

The dimensions of video sequences I^e , I^s , and v are all set to be $3 \times 3 \times 128 \times 256$ (*time* \times *channel* \times *height* \times *width*). In order to make them compatible with 2D CNNs, we combine the time dimension with the channel dimension by reshaping each of the video sequence into a $9 \times 128 \times 256$ tensor. We adjust the kernel dimensions of the first and the last layer in the original HRNetV2-W18 accordingly to fit the dimension changes of the inputs and outputs.

Counterpart Method Implementations In order to make an apple-to-apple comparison, we replace the backbone networks in different variational video prediction approaches with the same HRNet and remain the original prediction and training framework. We set β to 2 in β -VAE and employ a sine function ($0 - \frac{\pi}{2}$) as the anneal curve in Anneal-VAE. All the other training strategies are kept identical to VAE².

81 Training, Inference, and Implementation Details.

82 **Training.** I^e and v are concatenated along the channel dimension and fed into the encoder ϕ to
 83 generate two $64 \times 1 \times 1$ vectors that represent the mean \mathbf{m} and variance \mathbf{var} of the hidden code \mathbf{z} ,
 84 respectively. The code \mathbf{z} is then sampled according to the Gaussian distribution $\mathcal{N}(\mathbf{z}; \mathbf{m}, \mathbf{var})$. The
 85 encoder ψ takes as the inputs \mathbf{z} and I^e to generate the transition state I^s . Then, I^s and \mathbf{z} are fed into
 86 decoder θ' and θ together to reconstruct I^e and v with L1 loss, respectively. Meanwhile, I^s are passed
 87 into the discriminator D_ω to obtain adversarial gradients, where D_ω is learned by distinguishing the
 88 samples generated from the encoder ψ and the samples from the real dataset. Please note that, for the
 89 encoder ψ , we employ an extra noise signal drawn from a normal distribution which has the same
 90 size as \mathbf{z} to generate different I^s for the adversarial learning.

91 **Inference.** we sample the hidden code \mathbf{z} multiple times according to $\mathcal{N}(\mathbf{z}; \mathbf{0}, \mathbf{I})$. For each sampled \mathbf{z} ,
 92 we concatenate it with observation I^e and feed them into encoder ψ to generate I^s . Then I^s together
 93 with \mathbf{z} is fed into decoder θ to predict the corresponding v .

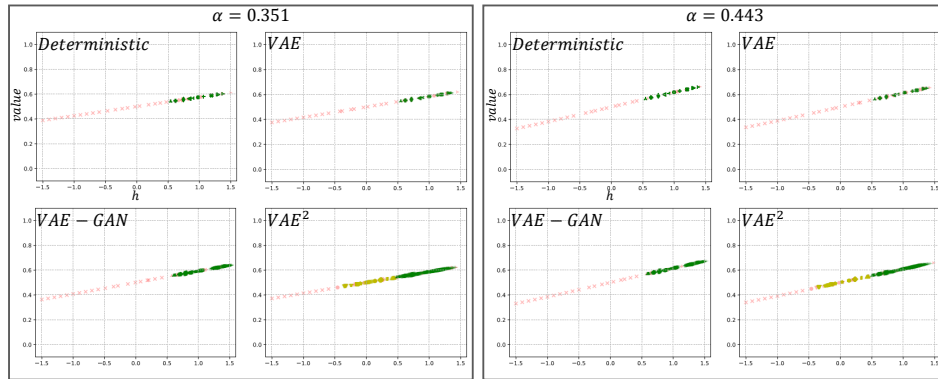
94 **Data Augmentation.** we randomly select nine consecutive frames from a video sequence for I^e , I^s ,
 95 and v , respectively. We resize the spatial dimension to 128×256 without random cropping or color
 96 jittering.

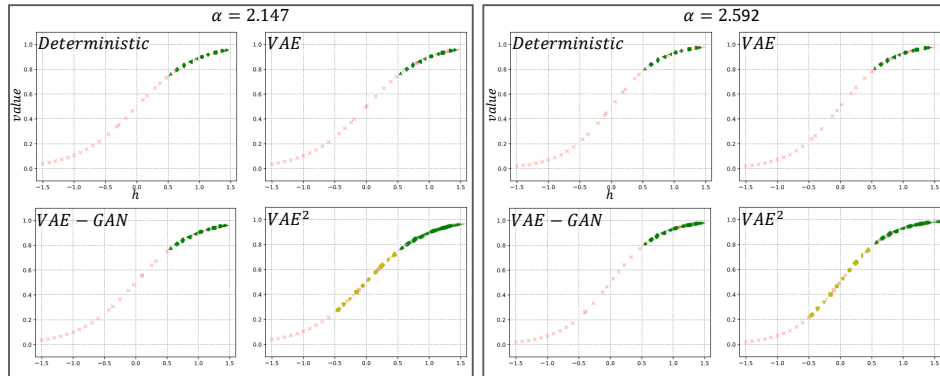
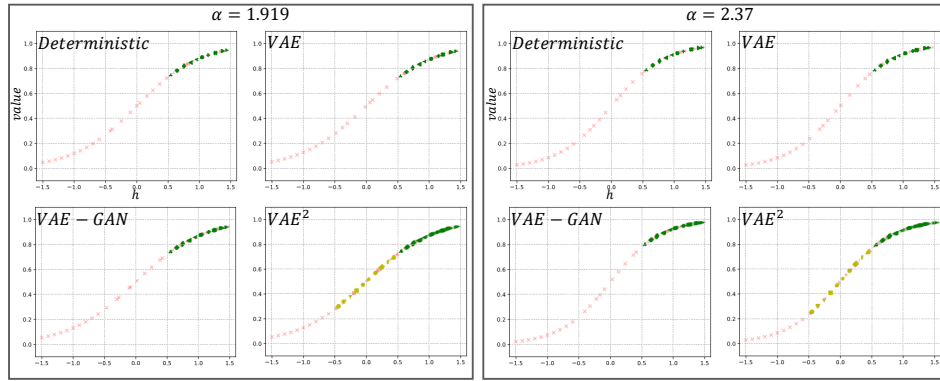
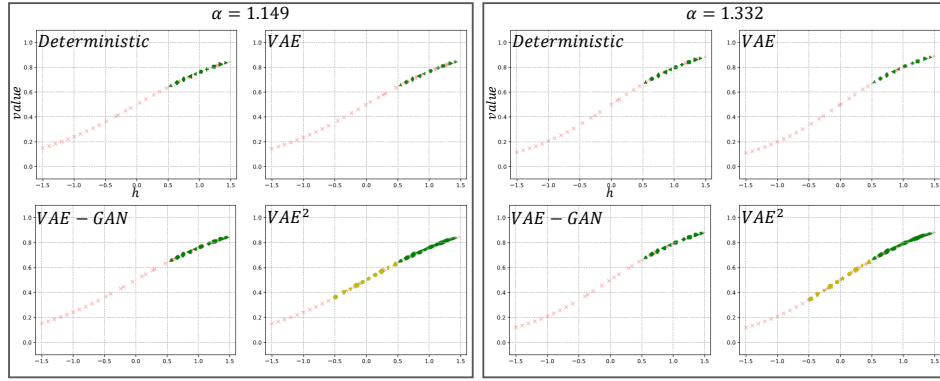
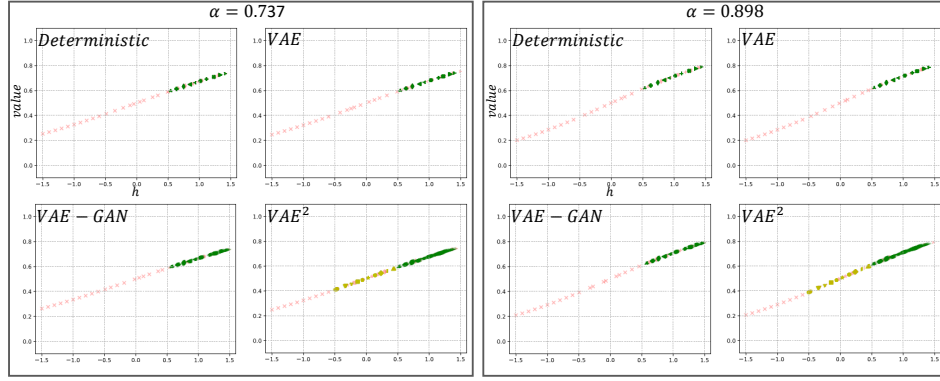
97 **Hyper-parameter.** In order to be comparable with the previous works, the prior distribution for
 98 the latent code \mathbf{z} is set to be $\mathcal{N}(\mathbf{z}; \mathbf{0}, \mathbf{I})$ without further tuning. We use Adam optimizer to train all
 99 methods for 1,000 epochs on the official train/validation split provided by the Cityscapes. The weight
 100 decay is set to $1e^{-4}$ and the initial learning rate is $1e^{-3}$. The λ is set to 0.1, which is decided by the
 101 grid search from 0.01 to 1. We observe that λ larger than 0.3 makes the generated transition state
 102 I^s decay to the partial observation I^e , while λ smaller than 0.05 makes the I^s decay to the future
 103 v . We also re-scale the adversarial loss of D_ω by multiplying 0.1 to enable a more stable training
 104 process. We leverage 8 Nvidia V100 GPUs (32G memory version) and distributed training strategy
 105 with batch size 32 and Synchronized Batch Normalization activated. During parameter tuning, we
 106 find that extra supervision on I^s at early training stages makes the whole framework converge faster
 107 and in a more stable way. Therefore, in addition to the objective function eq. (6) in the paper, we add
 108 an L1 loss between I^s generated by the encoder ψ and the ground-truth provided in the dataset with a
 109 small coefficient (0.05).

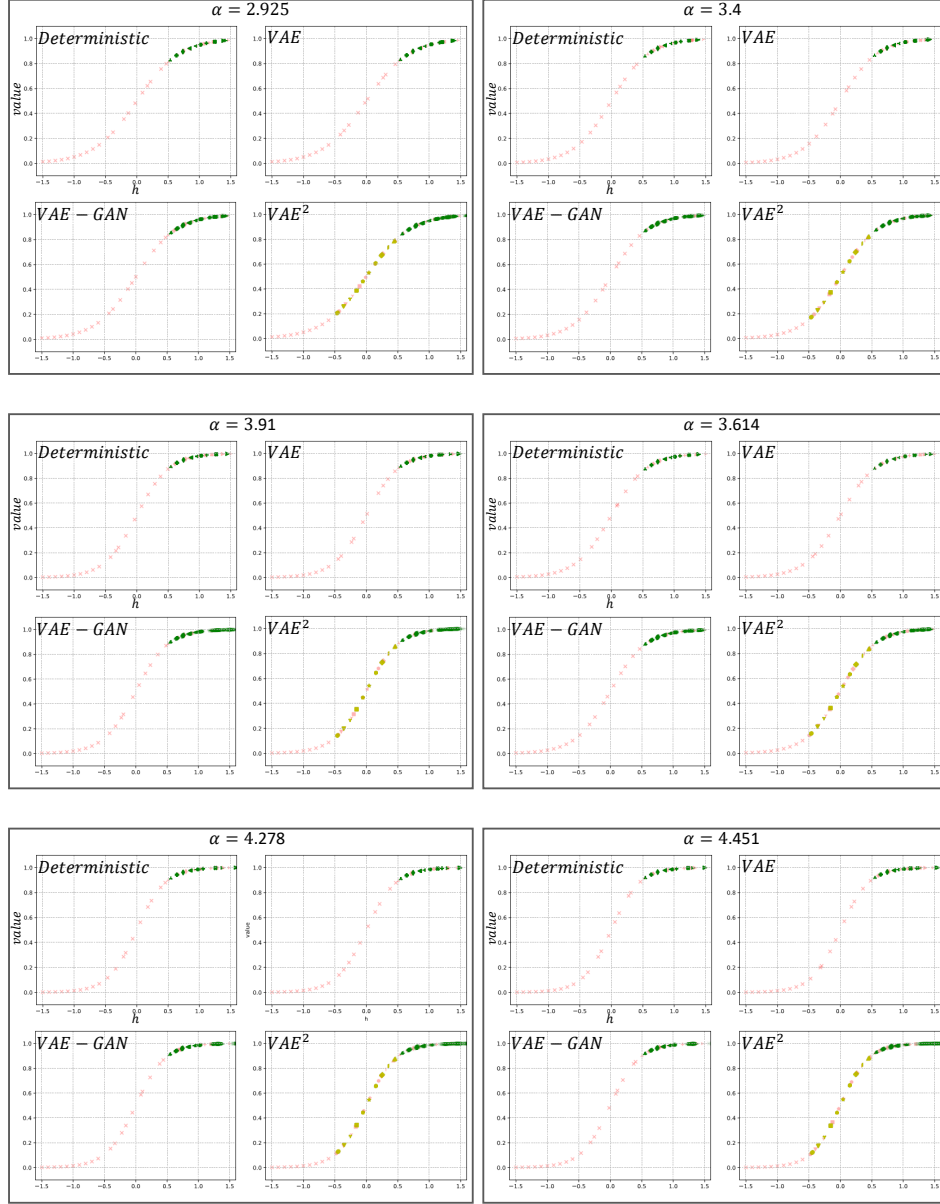
110 3 Visualization

111 3.1 Number Sequence Prediction

112 We provide more visualizations as a supplement to the Section 4 in the paper.







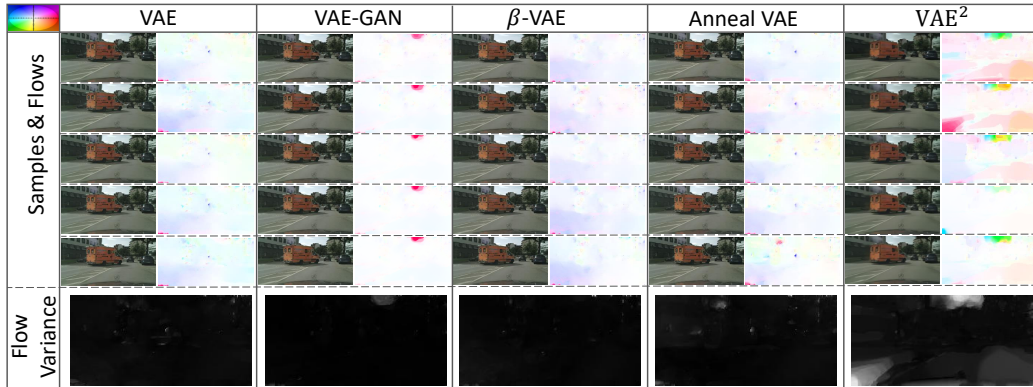
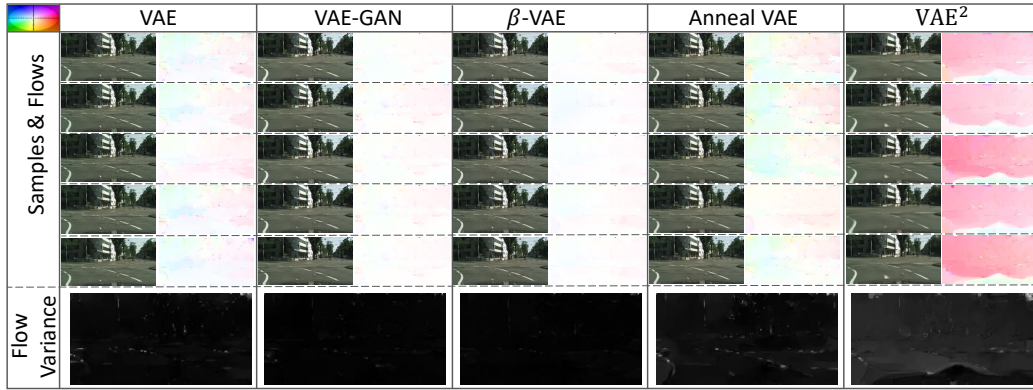
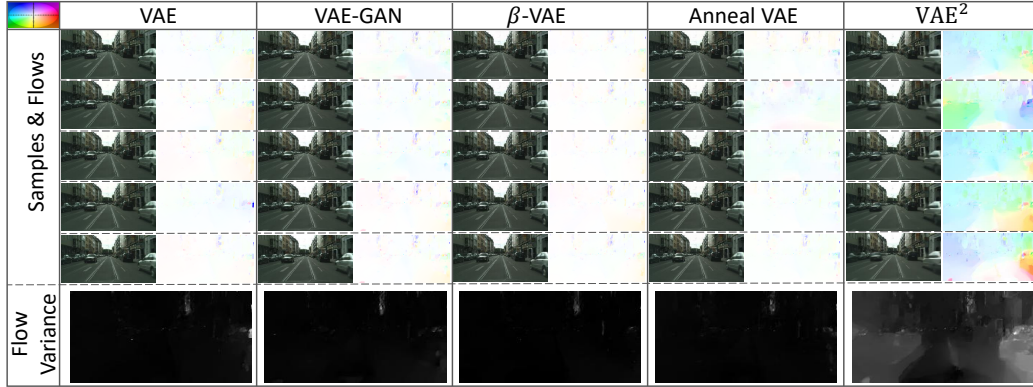
113 3.2 Multi-future Predictions on Cityscapes





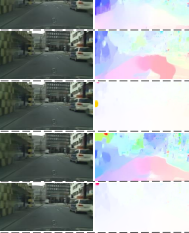





114 We provide more visualizations as a supplement to the Section 5.4 in the paper. The flow variance
 115 map is normalized to 0-255, where the highest standard deviation under one visualization group is
 116 set to 255. One figure corresponds to one group. The region with higher flow variance indicates the
 117 predicted content on this region from different samples is more diverse.











	VAE	VAE-GAN	β -VAE	Anneal VAE	VAE ²
Samples & Flows					
Flow Variance					

	VAE	VAE-GAN	β -VAE	Anneal VAE	VAE ²
Samples & Flows					
Flow Variance					

	VAE	VAE-GAN	β -VAE	Anneal VAE	VAE ²
Samples & Flows					
Flow Variance					

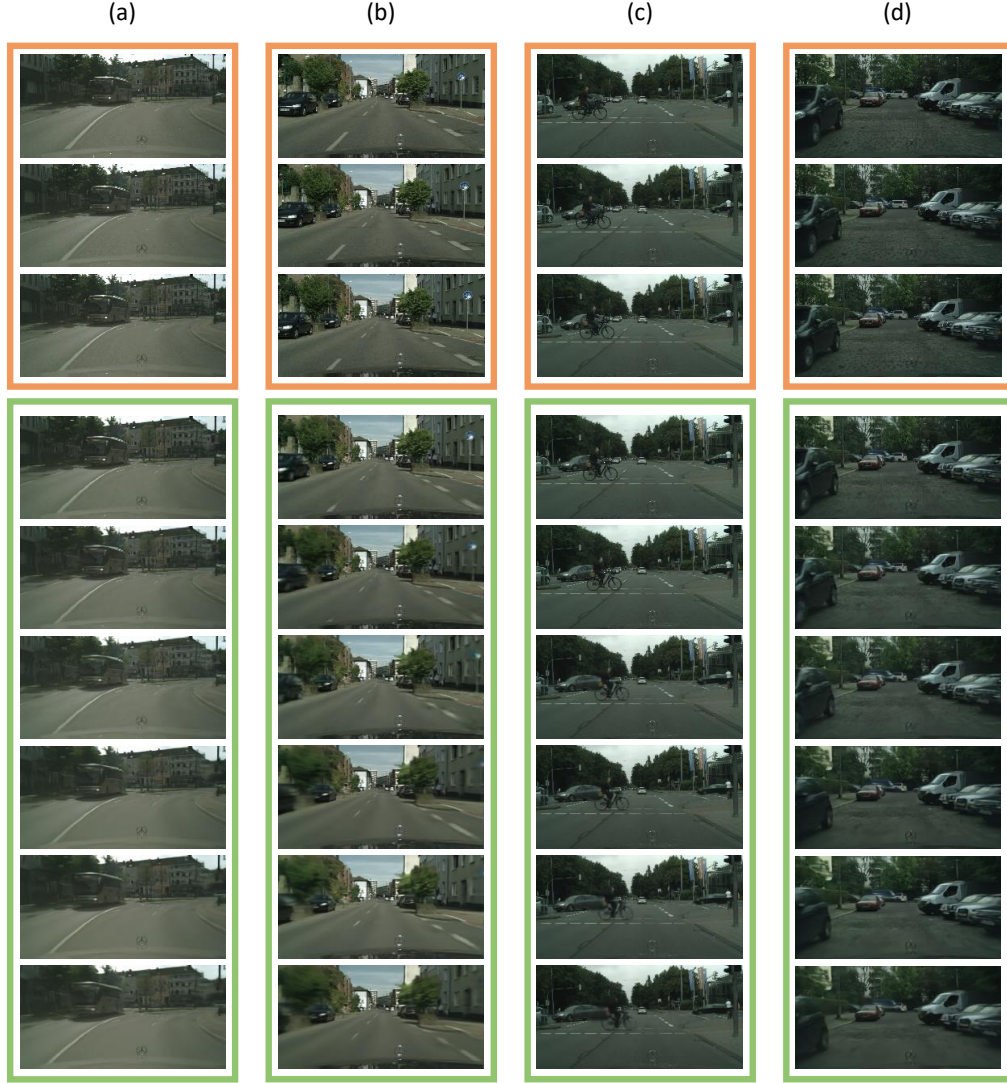


	VAE	VAE-GAN	β -VAE	Anneal VAE	VAE ²
Samples & Flows					
Flow Variance					

	VAE	VAE-GAN	β -VAE	Anneal VAE	VAE ²
Samples & Flows					
Flow Variance					

118 3.3 Multi-step Predictions on Cityscapes

119 We use VAE² to predict six future frames in an auto-regressive way, where the predicted future in
 120 each step is employed as new observation. We randomly select 12 sequences for visualization in
 121 the figures below. The orange and green bounding boxes denote the observation and prediction,
 122 respectively. As can be viewed from the figures, the futures predicted by VAE² provide very natural
 123 and recognizable content. Here we only visualize one of many possible sequences. In fact, if we
 124 choose different predicted futures as new observations, a huge amount different future sequences can
 125 be generated. For better illustration, we visualize 100 possibilities of the fourth predicted future in
 126 each sequence with GIF animation. Please find the corresponding GIF files in the supplementary
 127 materials.



(e)



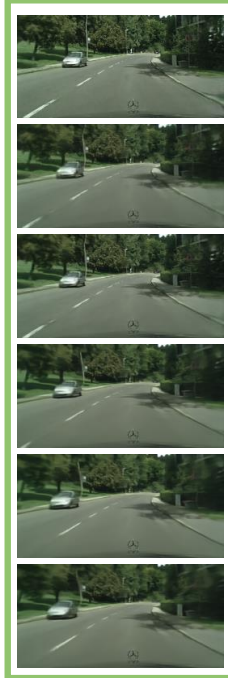
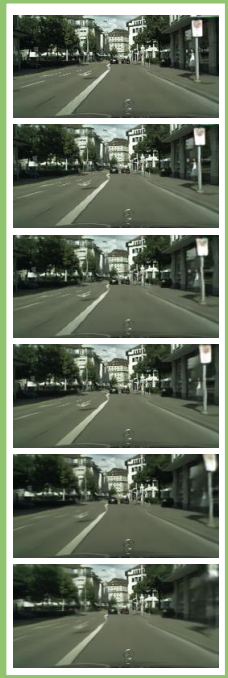
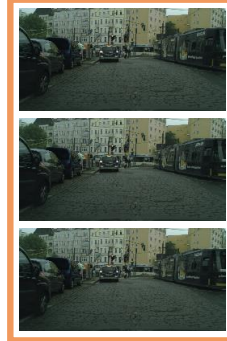
(f)



(g)



(h)



(i)



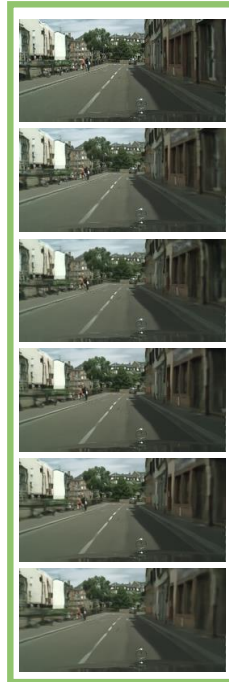
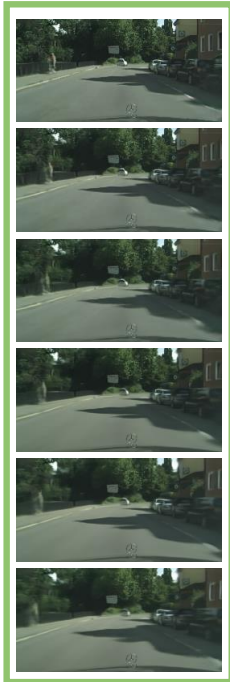
(j)



(k)



(l)



References

- [1] Diederik P Kingma and Max Welling. Auto-encoding variational bayes. *arXiv preprint arXiv:1312.6114*, 2013.
- [2] Andrew L Maas, Awni Y Hannun, and Andrew Y Ng. Rectifier nonlinearities improve neural network acoustic models. In *Proc. icml*, volume 30, page 3, 2013.
- [3] Ke Sun, Bin Xiao, Dong Liu, and Jingdong Wang. Deep high-resolution representation learning for human pose estimation. In *Proceedings of the IEEE Conference on Computer Vision and Pattern Recognition*, pages 5693–5703, 2019.
- [4] Jingdong Wang, Ke Sun, Tianheng Cheng, Borui Jiang, Chaorui Deng, Yang Zhao, Dong Liu, Yadong Mu, Minghui Tan, Xinggang Wang, et al. Deep high-resolution representation learning for visual recognition. *IEEE transactions on pattern analysis and machine intelligence*, 2020.
- [5] Kaiming He, Xiangyu Zhang, Shaoqing Ren, and Jian Sun. Deep residual learning for image recognition. In *Proceedings of the IEEE conference on computer vision and pattern recognition*, pages 770–778, 2016.